International Journal of Bifurcation and Chaos

Nonholomorphic singular continuation: a case with radial symmetry

Submitted October 15, 2012

Brett Bozyk
Department of Mathematics and Statistics, University of Minnesota Duluth
Duluth, MN 55812 USA
bozyk002@d.umn.edu

Bruce B. Peckham
Department of Mathematics and Statistics, University of Minnesota Duluth
Duluth, MN 55812 USA
bpeckham@d.umn.edu

Received (to be inserted by publisher)

This paper is a study of special families of rational maps of the real plane of the form:

$$z \mapsto z^n + c + \beta/\overline{z}^d,$$

where the dynamic variable $z \in \mathbb{C}$, and $\mathbb{C}$ is identified with $\mathbb{R}^2$. The parameters c and β are complex; n and d are positive integers. For β small, this family can be considered a non-holomorphic singular perturbation of the holomorphic family $z \mapsto z^n + c$, although we will consider large values of β as well. We focus on the special case where $n = d$ and $c = 0$ because the radial component of these maps in polar coordinates decouples from the angular component. This reduces a significant part of the analysis to the study of a family of one-dimensional unimodal maps. For each fixed n, the β parameter plane separates into three major regions, corresponding to maps which have one of the following behaviors: (i) all orbits go off to infinity, (ii) only an annulus of points stays bounded, and (iii) only a Cantor set of circles stays bounded. In cases (ii) and (iii), there is a transitive invariant set; this set is an attractor in case (ii). The dynamics of $z^n + \beta/\overline{z}^n$ is compared and contrasted to the (holomorphic) singularly perturbed maps: $z \mapsto z^n + \lambda/z^n$, studied by Devaney and coauthors over the last decade. Additional observations, mostly numerical, are made about the cases where $c \neq 0$ and $n \neq d$.

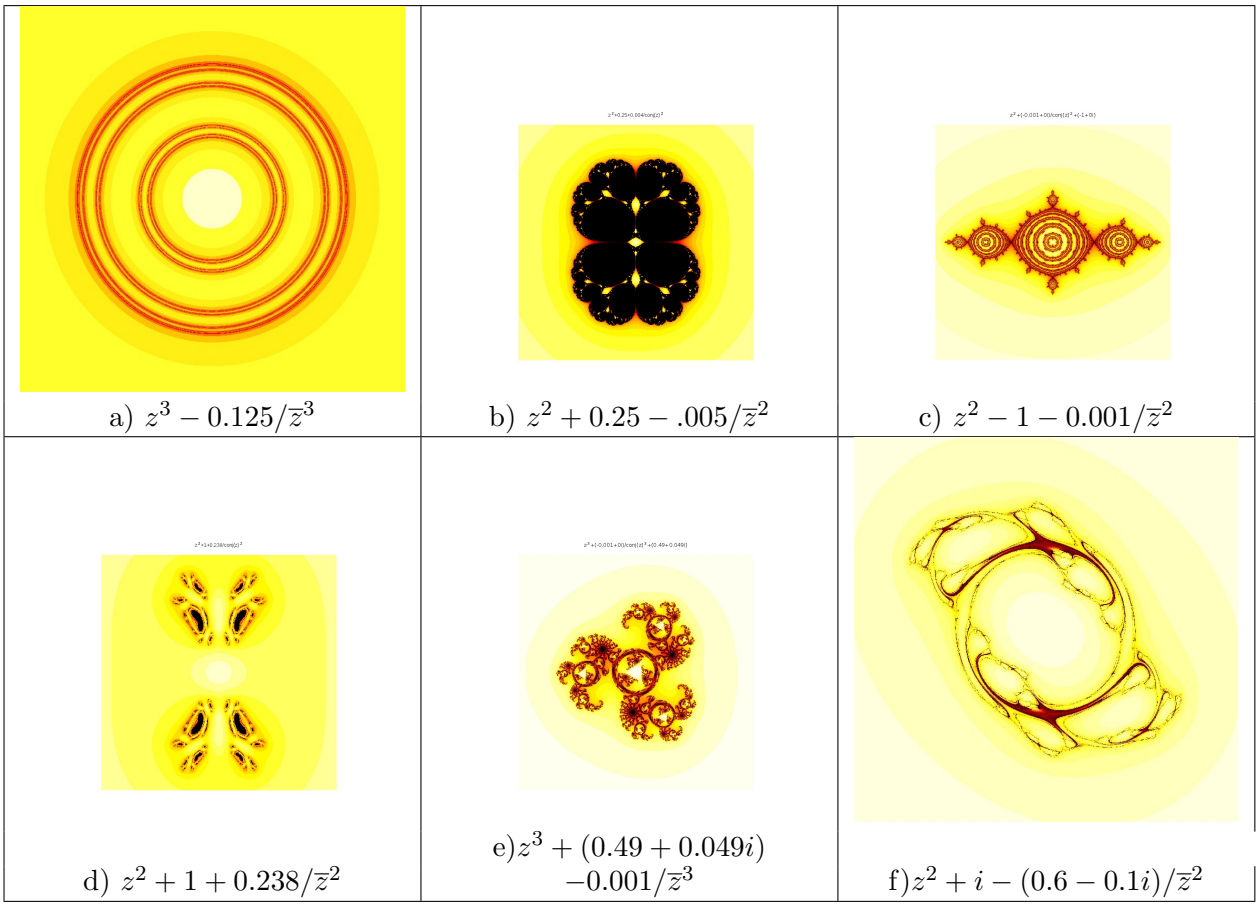

Fig. 1. Examples of escape/nonescape sets in the dynamic plane (z) for maps in the form of eq. (1). Coloring matches standard algorithms for filled Julia sets: black indicates initial conditions corresponding to bounded orbits, other colors indicate escape to infinity, with shading indicating the number of iterates to satisfy the escape criterion, lighter shading indicating fewer iterates.

1. Introduction

Rational holomorphic maps of the complex plane $\mathbb{C}$ (or the Riemann sphere $\hat{\mathbb{C}}$) form a very special subset in the more general function space of rational maps of the real plane $\mathbb{R}^2$ (or the one-point compactification obtained by adding the point at infinity, which we denote by $\hat{\mathbb{R}^2}$). Although the study of bifurcations of iterated maps in the two settings has overlap, the reliance on powerful theorems in the holomorphic setting makes the two areas seem, in some respects, to be completely distinct areas of research. In this paper, we provide a connection between the two areas by investigating the dynamics of maps of the form

$$F_{(n,d,c,\beta)}(z,\overline{z}) = z^n + c + \beta/\overline{z}^d. \tag{1}$$

The powers n and d are positive integers, and c and β are complex parameters. We shall represent β in rectangular form as $\beta = \beta_1 + \beta_2 i$ and in polar form as $\beta = |\beta|e^{i\phi}$, so $\phi = \arg(\beta)$. We study the dynamics and associated bifurcations for the maps in this family. When $\beta = 0$, we have a holomorphic map $z^n + c$. Thus, for small β, this family can be considered as a (singular) perturbation of a holomorphic map of the complex plane. The dynamics of $z^n + c$ is well-studied, especially when $n = 2$ or $c = 0$, so this gives us a basis for comparison. It also allows us to focus on a certain subset of rational maps of the plane – in the form of eq.(1), avoiding the very difficult task of describing the dynamics of all rational maps of the real plane.

Since infinity is attracting for all maps in this family, the simplest starting point for a dynamical study can be performed by numerically investigating orbits that are bounded versus those that escape to infinity. Several dynamic plane pictures of the initial conditions corresponding to bounded orbits are

shown in Fig. 1. Understanding these pictures, as well as the dynamics restricted to the set of bounded orbits, is a general goal of the study, but in this paper we focus mostly on the case where $n = d$ and $c = 0$: $F_{(n,n,0,\beta)}(z, \overline{z}) = z^n + \beta/\overline{z}^n$. In this restricted family, the radial coordinate of the dynamics in polar coordinates decouples, reducing much of the study to that of a family of negative Schwarzian unimodal maps of an interval. This radial family behaves much like the real one-dimensional family $x^2 + c$, with the collection of radii having bounded orbits falling into one of three categories: the empty set (analogous to $c > 0.25$), an interval containing a transitive "topological attractor" ($-2.0 \leq c \leq 0.25$), or a Cantor set on which the dynamics is conjugate to the shift on two symbols ($c < -2.0$). Consequently, the set of initial conditions corresponding to bounded orbits for the full planar maps can be empty, an annulus (look ahead to Fig. 12(a)), or a Cantor set of circles (Fig. 1(a)). We show in this paper that when the radial map has a chaotic attractor, that the full map of the plane also has a chaotic attractor which is the radial attractor crossed with the circle $\mathbb{S}^1$.

In the β parameter plane, for every integer $n \geq 2$, the region corresponding to an annulus of bounded orbits is a "parabolic strip", with all orbits escaping for parameter values to the right of this strip, and a Cantor set of circles staying bounded for parameter values to the left. Look ahead to the bifurcation diagrams in figures 3 and 7 for $n = 3$ and $n = 2$, respectively. Bifurcation curves inside the parabolic region are roughly parallel for $n \geq 3$, but are more interesting geometrically near $\beta = 0$ for $n = 2$. This is consistent with the fact that $n = 2$ is special for the family $z^2 + \gamma/z^2$ [Devaney, 2012]. The case $n = 1$ also has some unique properties, such as failing to have regions corresponding to $c < -2$.

The organization of the paper is as follows. Section 2 holds some general results for all families of the form of eq. (1). The main analytical results are in Sec. 3, where we restrict the study to $z^n + \beta/\overline{z}^n$. Included in that section is an analysis of the dynamics of the radial maps, the full planar maps, and a brief comparison of the dynamics of our maps to the dynamics for *holomorphic* singular continuations, $z^n + \lambda/z^n$. Some generalizations are suggested in Sec. 4.

The work in this paper complements and extends ideas from previous studies of nonholomorphic (but nonsingular) continuations of holomorphic maps [Drexler, 1996; Peckham, 1998; Peckham & Montaldi, 2000; Bielefeld, et al.; Bruin & van Noort, 2004], and singular (but holomorphic) continuations of holomorphic maps [Devaney, 2010, 2012; Devaney *et al.*, 2005; Blanchard *et al.*, 2005, 2012]. Many of the results in the paper appeared as part of the first author's master's thesis [Bozyk, 2012].

2. Preliminaries

2.1. *Escape criterion*

It is well-known that infinity is a superattracting fixed point for $z^n + c$ for any $n \geq 2$ and $c \in \mathbb{C}$, so it should not be surprising that infinity is still attracting for maps in the form of eq. (1). To find an explicit escape radius, we establish the following escape criterion.

Theorem 1. *Assume* $n \geq 2$. *If* $|z| > \max\left\{4^{1/(n-1)}, |\beta|^{1/(d+1)}, |c|\right\}$, *then* $|F_{n,d,c,\beta}(z)| > 2|z|$.

Proof. Since $|z| > 4^{1/(n-1)}$, $|z|^{n-1} > 4$, so $|z|^n > 4|z|$; since $|z| > |\beta|^{1/(d+1)}$, $|\beta/\overline{z}^d| < |z|$. The triangle inequality then implies:

$$|F_{n,d,c,\beta}(z)| = |z^n + c + \beta/\overline{z}^d| \geq |z|^n - |c| - |\beta/\overline{z}^d| > 4|z| - |z| - |z| = 2|z|.$$

■

This escape criterion could clearly be improved by requiring $|F(z)| > a|z|$ with $a < 2$ but still greater than 1. This theorem, however, is sufficient for our numerical experiments.

2.2. *Symmetry*

There is an obvious symmetry relating conjugate parameters: $F_{n,d,\overline{c},\overline{\beta}}(\overline{z}) = \overline{F_{n,d,c,\beta}(z)}$. This implies that maps with conjugate parameters with have conjugate dynamic space behavior. In the case where c is real,

this will require β parameter space diagrams, when all other parameters are fixed, to be symmetric about the real axis. A similar symmetry can be verified to be $F_{n,d,ce^{in\omega},\beta e^{i(n-d)\omega}}(ze^{i\omega}) = F_{n,d,c,\beta}(z)e^{in\omega}$. This has consequences for certain choices of ω, especially when $c = 0$ or $n = d$, but we shall not investigate them fully here. When both $c = 0$ and $n = d$, this gives $F_{n,d,0,\beta}(ze^{i\omega}) = F_{n,d,0,\beta}(z)e^{in\omega}$, which shows the radial decoupling which we will obtain by more direct computation in Sec. 3.

2.3. *Coordinates*

Our family in eq. (1) is written in $(z, \overline{z})$ coordinates. This can be converted into standard rectangular coordinates in the usual way: $z = x + iy \in \mathbb{C} \leftrightarrow (x, y) \in \mathbb{R}^2$; $\overline{z} = x - iy$. Similarly, $F(z) \in \mathbb{C} \leftrightarrow (\mathrm{Re}(F(z)), \mathrm{Im}(F(z))) \in \mathbb{R}^2$.

The Jacobian matrix can be computed directly in (x, y) coordinates, but the use of "$(z, \overline{z})$ coordinates provides a computational shortcut. We view z and $\overline{z}$ as independent complex coordinates, think of $F(z)$ as $F(z, \overline{z})$, and extend the map F to $(F, \overline{F})$, where $\overline{F}(z, \overline{z}) \equiv \overline{F(z, \overline{z})}$. For our model family in eq. (1), $\overline{F}(z, \overline{z}) = \overline{z}^n + \overline{c} + \frac{\overline{\beta}}{z^d}$. The Jacobian matrix is the 2×2 matrix $\frac{\partial(F,\overline{F})}{\partial z \partial \overline{z}}$. We will use this in our computation of "critical sets" below. (This computation is justified by starting with $(x, y) \in \mathbb{R}^2$, complexifying to view $(x, y) \in \mathbb{C}^2$, performing the change of variables from $(x, y) \in \mathbb{C}^2$ to $(z, w) \in \mathbb{C}^2$ defined by $x = (z + w)/2$ and $y = (z - w)/(2i)$, and noticing that restricting x and y to be real is equivalent to setting $w = \overline{z}$.)

2.4. *Critical Sets*

For rational (holomorphic) maps of $\hat{\mathbb{C}}$, it has been well-established that the critical orbits play a key role in determining the dynamics of all orbits. The same thing is true for maps of $\mathbb{R}^2$. (See [Mira & Narayaninsamy, 1993], for example.) In these maps, the critical set, denoted J_0 in the literature, is defined by the dynamic space points for which the Jacobian determinant is zero.

Proposition 1. *The critical set J_0 for family $F_{n,d,c,\beta}$ is a circle of radius*

$$r = \left(\frac{d}{n}|\beta|\right)^{\frac{1}{n+d}}.$$

Proof. This follows from a direct computation of the Jacobian determinant. Using the $(z, \overline{z})$ coordinates as suggested in subsection 2.3, the Jacobian determinant becomes $\frac{\partial(F,\overline{F})}{\partial z \partial \overline{z}} = \begin{pmatrix} nz^{n-1} & -\beta d\overline{z}^{-d-1} \\ -\overline{\beta} dz^{-d-1} & n\overline{z}^{n-1} \end{pmatrix}$. Setting the Jacobian determinant equal to zero results in $n^2|z|^{2n-2} - d^2|\beta|^2 \frac{1}{|z|^{2d+2}} = 0$. Letting $z = re^{i\theta}$, taking square roots, and solving for r results in the desired formula. ■

3. Case with radial symmetry: $n = d$ and $c = 0$

The main results of the paper are in this section. We restrict the general family $F_{n,d,c,\beta}$ of eq. (1) by setting $c = 0$ and $n = d$. We will denote such maps $F_{n,n,0,\beta}$ as $F_{n,\beta}$. The maps now takes the form

$$F_{n,\beta}(z) = z^n + \frac{\beta}{\overline{z}^n} \tag{2}$$

Substituting $z = re^{i\theta}$, eq. (2) becomes:

$$F_{n,\beta}\left(re^{i\theta}\right) = \left(re^{i\theta}\right)^n + \frac{\beta}{(re^{-i\theta})^n} = \left(r^n + \frac{\beta}{r^n}\right)e^{in\theta} = \left(r^n + \frac{\beta_1}{r^n} + i\frac{\beta_2}{r^n}\right)e^{in\theta} \tag{3}$$

where $\beta = \beta_1 + i\beta_2$. From this form it is clear that the radial component decouples from the angular component. We compute the polar coordinate version of eq. (2), which we will call $P_{n,\beta}$, to be:

$$P_{n,\beta}\begin{pmatrix} r \\ \theta \end{pmatrix} = \begin{pmatrix} \mathcal{M}_{n,\beta}(r) \\ \mathcal{A}_{n,\beta}(r,\theta) \end{pmatrix} = \begin{pmatrix} \sqrt{r^{2n} + 2\beta_1 + \frac{\beta_1^2+\beta_2^2}{r^{2n}}} \\ n\theta + Arg\left(r^n + \frac{\beta}{r^n}\right) \end{pmatrix}. \tag{4}$$

We call the radial component $\mathcal{M}_{n,\beta}$ the *modulus map*, and $\mathcal{A}_{n,\beta}$ the *angular map*. Studying the dynamics of $P_{n,\beta}$ is the main goal of this paper. $P_{n,\beta}$ and $F_{n,\beta}$ are, of course, dynamically conjugate. We have the usual polar coordinate identifications that $(0,\theta)$ is the origin for any θ, and (r,θ) is identified with $(r,\theta+2\pi)$.

3.1. *The modulus map*

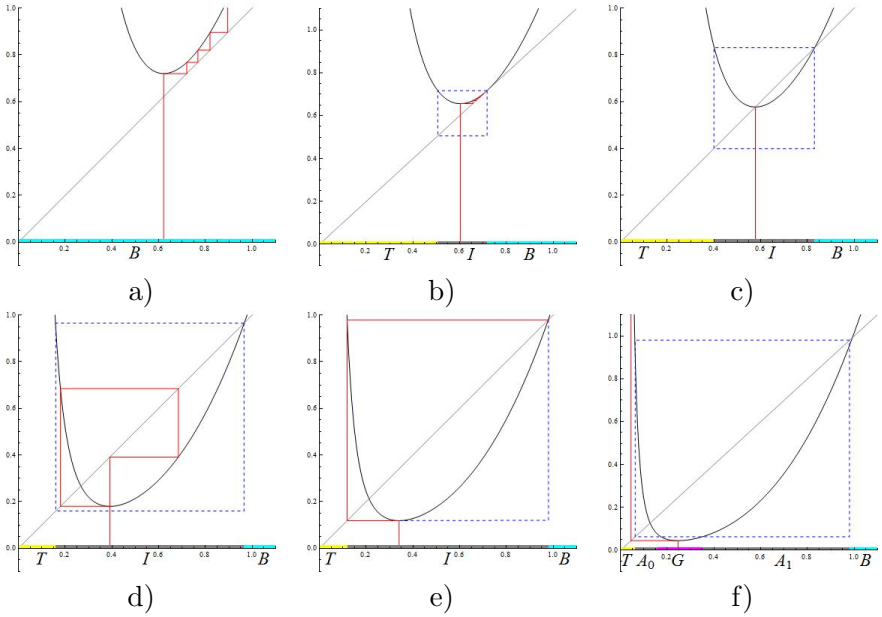

Fig. 2. Six graphs and critical orbits for $\tilde{\mathcal{M}}_{3,\beta}$ for β values along the ray $\phi = \arg(\beta) = \pi/3$. Key β values are chosen to illustrate the universal period-doubling route to chaos. These points are highlighted on the image of the parameter plane for $n = 3$ below, in Figure 3b. The right-hand endpoint of the interval $I^{3,\beta}$, determined by the dashed boxes in b-f, is p_+, while the left-hand endpoint is $\tau(p_+)$. Notice that the behaviors indicated by the graphical iteration are the same as those for x^2+c. a) all orbits escape, b) saddle-node (tangent) bifurcation point, c) superattracting fixed point, d) superattracting period-three orbit, e) critical orbit prefixed (after two iterates), f) critical orbit escapes, Cantor set contained in $A_0 \bigcup A_1$ left bounded. Notation: B is (if extended to infinity) the immediate basin of infinity; T (in b-f) is the "trap door" [Devaney, 2010], mapping to B; G (only in f) maps to T; I is the invariant interval $I^{3,\beta}$.

In this section we study the modulus map $\mathcal{M}_{n,\beta}$ and a slighty simpler conjugate $\tilde{\mathcal{M}}_{n,\beta}$. Note that we can assume $\mathcal{M}_{n,\beta} : [0,\infty] \to [0,\infty]$ by defining $\mathcal{M}_{n,\beta}(\infty) = \infty$ and, for $\beta \neq 0$, $\mathcal{M}_{n,\beta}(0) = \infty$, to extend the domain and range to include ∞; $\mathcal{M}_{n,\beta}$ is continuous on $[0,\infty]$ (in the usual order topology). $\mathcal{M}_{n,\beta}$ is a unimodal map for all $n \geq 1$ and $\beta \neq 0$. Its unique critical point, which is a local minimum, can be easily computed to be $r = |\beta|^{1/2n}$.

In order to eliminate the square root in the formula for $\mathcal{M}$ in eq. (4), we conjugate via the homeomorphism $s = h(r) = r^2$, defined on $[0,\infty]$. This leads us to a conjugate map we call $\tilde{\mathcal{M}}_{n,\beta}$, abbreviated by $\tilde{\mathcal{M}}$ when the parameters are either not necessary to specify or clear by context, defined on $[0,\infty]$ by

$$\tilde{\mathcal{M}}_{n,\beta}(s) = h^{-1} \circ \mathcal{M}_{n,\beta} \circ h(s) = s^n + 2\beta_1 + \frac{\beta_1^2+\beta_2^2}{s^n} = s^n + 2|\beta|\cos(\phi) + \frac{|\beta|^2}{s^n}. \tag{5}$$

The $\tilde{\mathcal{M}}_{n,\beta}$ maps are still unimodal, with minimum at $s = |\beta|^{1/n}$, but they have the advantage of being smooth (even analytic) on $(0,\infty)$, even though $\mathcal{M}_{n,\beta}$ can fail to be differentiable at its critical point when the critical point maps to zero (when $\beta_1 < 0$ and $\beta_2 = 0$). In addition, the $\tilde{\mathcal{M}}_{n,\beta}$

maps are "negative Schwarzian", even though the $\mathcal{M}_{n,\beta}$ maps are not. This can be verified by recalling that the Schwarzian derivative $Sf(x) = \frac{f'''(x)}{f'(s)} - \frac{3}{2}\left(\frac{f''(s)}{f'(s)}\right)^2$, and computing and simplifying to obtain $S\tilde{\mathcal{M}}(s) = \frac{(1-n^2)(|\beta|^4+s^{4n})-2(1+5n^2)|\beta|^2 s^{2n}}{2s^2(|\beta|^2-s^{2n})^2}$. For $\beta \neq 0$, and any $n \geq 1$, this expression is negative for $s \in [0,\infty]$, as long as $s \neq |\beta|^{1/n}$, the unique critical point. This allows us to quote some powerful theorems from one-dimensional dynamics [Guckenheimer J, 1979; de Melo & van Strein, 1993; Kraft, 2012]. Specifically, each map $\tilde{\mathcal{M}}_{n,\beta}$ with $n \geq 2$ and $\beta \neq 0$ is topologically conjugate to $Q_c(x) = x^2 + c$ for some c. Since $\mathcal{M}$ is conjugate to $\tilde{\mathcal{M}}$, $\mathcal{M}_{n,\beta}$ is also conjugate to $x^2 + c$ for these β values. As we shall detail later in the section, the role of decreasing c for $x^2 + c$ can be played either by decreasing β_1 for any fixed β_2, by decreasing $|\beta|$ for any fixed ϕ other than π, or by increasing ϕ from 0 to π. Representative graphs of $\tilde{\mathcal{M}}$, with $n = 3$, located along a ray in the parameter plane, are shown below in Fig. 2.

We will use the following notation in the rest of the paper.

- The unique critical point: $c^{n,\beta}$; its iterates: $\tilde{\mathcal{M}}^j_{n,\beta}(c^{n,\beta}) = c^{n,\beta}_j$. When parameters are clear, notation is shortened to c^β_j or c_j.
- The critical itinerary: $s = (s_j)$ where $j = 0, 1, 2, ...$, and
$$s_j = \begin{cases} L : c^{n,\beta}_j < c^{n,\beta} \\ C : c^{n,\beta}_j = c^{n,\beta} \\ R : c^{n,\beta}_j > c^{n,\beta} \end{cases}$$
When the critical orbit is periodic of period q, we write its itinerary as $\overline{Cs_1s_2...s_{q-1}}$.
- The fixed points of $\tilde{\mathcal{M}}_{n,\beta}$ (when they exist): $p^{n,\beta}_- \leq p^{n,\beta}_+$. When parameters are clear, notation is shortened to p^β_+ or p_+.
- The "interval of interest": $I^{n,\beta} = [\tau(p^{n,\beta}_+), p^{n,\beta}_+]$, where τ maps a point in $[0,\infty]$ to its "companion point" having the same image under $\tilde{\mathcal{M}}_{n,\beta}$; note that $\tau(c^{n,\beta}) = c^{n,\beta}$. In particular, $\tilde{\mathcal{M}}_{n,\beta}(\tau(p^{n,\beta}_+)) = p^{n,\beta}_+$. This interval exists whenever $p^{n,\beta}_+$ exists; it is invariant if and only if $c^{n,\beta}_2 \leq p^{n,\beta}_+$ (equivalently $c^{n,\beta}_1 \geq \tau(p^{n,\beta}_+)$). See Fig. 2f where the interval is *not* invariant.
- $K(\tilde{\mathcal{M}}_{n,\beta})$ is the set of all initial conditions in $[0,\infty]$ for which the corresonding orbit remains bounded.
- $J(\tilde{\mathcal{M}}_{n,\beta}) = \partial K(\tilde{\mathcal{M}}_{n,\beta})$
- $K(F_{n,\beta})$ and $J(F_{n,\beta})$ are the analogous sets for the full map of eq. (1) in the plane. The notation is chosen to match the standard notation for the filled Julia sets and Julia sets, respectively, from complex dynamics. We caution the reader that the usual properties of filled Julia sets and Julia sets do not necessarily extend to real planar maps.
- PS_n is the subset of the β parameter plane for power parameter n for which the corresponding critical orbit is bounded. The notation is chosen to suggest either "parameter space", or "parabolic strip." This is analogous to the Mandelbrot set for complex quadratic maps.
- Bifurcation sets contained in PS_n in the β parameter plane: SNq_n, PDq_n, SAq_n, PFq_n represent, respectively, saddle-node, period-doubling, superatttracting, and prefixed parameter values for period-q and power parameter n. These sets are typically curves, or unions of curves in PS_n. Different period-q curves could be distinguished further by the critical itinerary, but we do not always do so in this paper.

3.1.1. *The β parameter plane for $n = 3$.*

We begin with a description of the $n = 3$ parameter plane. The parameter planes for $n > 3$ are topologically and geometrically similar. The parameter plane for $n = 2$ is almost the same topologically, but quite different geometrically, especially near $\beta = 0$. We will deal with the $n = 2$ geometry below. For completeness, $n = 1$ also is treated as a special case below.

A coarse division of the parameter plane is obtained by performing numerical escape experiments for the critical orbit in the β plane. The resulting "parabolic strip" is displayed in Fig. 3(a). A finer division is given by numerically computed bifurcation curves in the strip. One of the curves, the superattracting

fixed-point curve, denoted $SA1_3$, has an explicit formula which we give in eq. (7) for general n below. The results are displayed in Fig. 3(b).

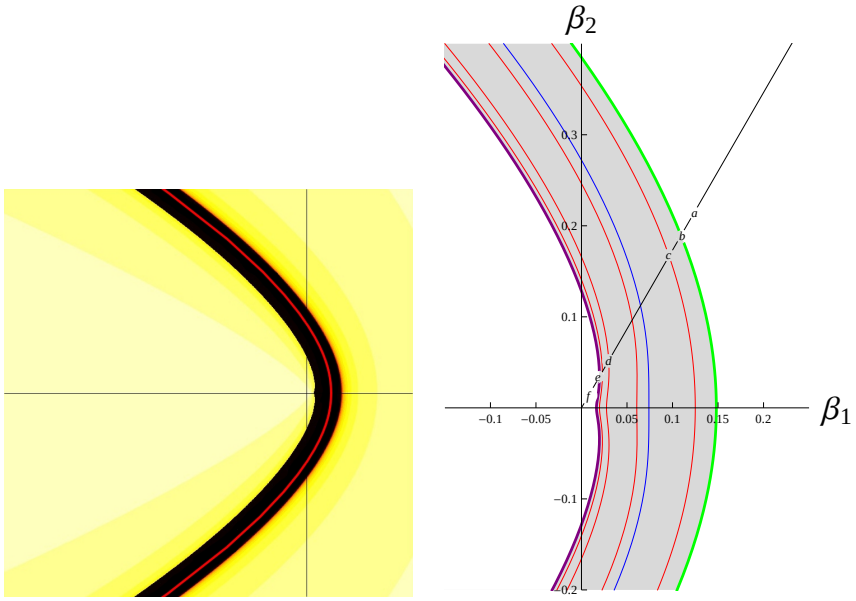

a) b)

Fig. 3. The parabolic strip PS_3 in the β parameter plane for $\tilde{\mathcal{M}}_{3,\beta}$. a) Escape experiments: black corresponds to bounded critical orbits; colored regions correspond to escaping critical orbits, with lighter colors having faster rates of escape. The red curve of superattracting fixed points is traced out by the polar coordinate curve: $|\beta| = 1/(2(1+\cos(\phi)))^{3/2}$; $\beta \in [-2.5, 0.5] \times [-1.5, 1.5]\,i$. b) An enlargement showing several numerically computed bifurcation curves in the parabolic strip; shown are, right to left, the fixed-point saddle-node right-hand boundary of the strip (green), the fixed-point superattracting curve $SA1_3$ (red), the fixed-point period-doubing curve (blue), the period-$2, 3, 4$ superattracting curves $SA2_3$, $SA3_3$, $SA4_3$ (all red), and prefixed point curve on the left-hand boundary (purple). (Note that the period-k superattracting curves are not unique for $k \geq 4$ since, for these k, there are multiple "period-k windows" for $x^2 + c$.) Along the ray $\phi = \pi/3$ are the six parameter values a-f whose graphical iterations are displayed in Figure 2.

The boundaries of the nonescape region PS_3 were numerically confirmed by continuing [Peckham, 1988-2012] the right-hand boundary as a fixed-point saddle-node curve, and the left-hand boundary as a prefixed point curve ($c_2^{n,\beta} = p_+^{n,\beta}$). (The prefixed points are also classified as degenerate homoclinic points [Devaney, 1986].) We show several graphical iteration diagrams for parameter values along a "$\pi/3$" ray. See the ray in Fig. 3, and the corrreponding graphs and iterations in Fig. 2.

For β values to the right of the strip, all orbits escape to infinity monotonically (not just the critical orbit); for β values in the black parabolic strip, only the invariant interval $I^{3,\beta} = [\tau(p_+^{3,\beta}), p_+^{3,\beta}]$ stays bounded; for β values to the left of the strip, the critical orbit escapes to infinity (monotonically *after* the first iterate), but a Cantor set of s values stays bounded. This is analogous to the behavior of iterations of $x^2 + c$, where for $c > 1/4$, all orbits go off to infinity, for $-2 < c < 1/4$, only a closed interval stays bounded, and for $c < -2$, a Cantor set of points stays bounded. Numerically, it appears that crossing the parabolic strip from right to left in any of the following ways corresponds to decreasing c from $1/4$ to -2 for the quadratic family $x^2 + c$: along a ray to the origin, horizontally by decreasing β_1, or on a constant $|\beta|$ circle from $\phi = 0$ to $\phi = \pi$ (for $|\beta| > \beta_1^{sn}$, where β_1^{sn} is the saddle-node parameter value on the β_1 axis; see Fig. 3b where β_1 is seen to be approximately 0.15. More generally, any curve passing through both boundaries of PS_3 is a "full family"

3.1.2. *The β parameter plane for $n > 3$.*

Numerical investigation suggests that the geometry of the β parameter planes for $n > 3$ is qualitatively similar to the geometry of the $n = 3$ parameter plane: the strip boundaries and all of the interior bifurcation

curves are roughly parallel. As n increases, the width of the strip shrinks toward zero. The strips and all the bifurcation curves in it limit to the same parabola: $x = -y^2 + 1/4$. See Figures 4 and 5. This statement is supported by the following arguments.

The critical orbit. Straightforward computation using the map definition in eq. (5) shows the first two iterates of the critical orbit are:

$$|\beta|^{1/n} \mapsto 2|\beta|(1+\cos(\phi)) \mapsto (2|\beta|(1+\cos(\phi)))^n + 2|\beta|\cos(\phi) + \frac{|\beta|^2}{(2|\beta|(1+\cos(\phi)))^n} \tag{6}$$

Note that when $\phi = \pi$, the critical value is zero, and the second iterate is infinity.

The parabolic superattracting fixed point limit as $n \to \infty$. The superattracting fixed point parameter set $SA1_n$ (maps conjugate to $x^2 + 0$) can be explicitly expressed parametrically in polar coordinates by requiring the critical point $|\beta|^{1/n}$ to be mapped to itself using eq. (6), and solving for $|\beta|$. The result is:

$$SA1_n = \left\{ |\beta|e^{i\phi} : |\beta| = \left(\frac{1}{2(1+\cos(\phi))} \right)^{\frac{n}{n-1}} \right\} (\phi \neq \pi) \tag{7}$$

As $n \to \infty$, $\frac{n}{n-1}$ limits to 1, and the above equation is the polar coordinate version of the parabola $x = -y^2 + 1/4$. See Fig. 4.

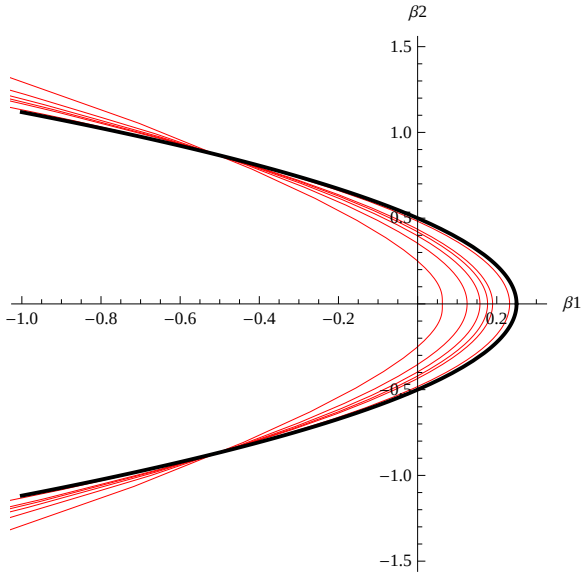

Fig. 4. Superattracting fixed point parameter curves for powers $n = 2, 3, 4, 5, 6, 20$, left to right as they intersect along the β_1 axis, and the limiting parabola (black) as $n \to \infty$. The curves all pass through $(|\beta|, \phi) = (1, \pm\frac{2\pi}{3})$.

Width of the strip decreases as $n \to \infty$. For this argument, we provide only framework of a proof. We will consider what happens as we approach the origin along a fixed ray $\arg(\beta) = \phi$. Passing through the strip is analogous to decreasing c in $x^2 + c$ from 0.25 to -2.0. That is, the graph of $\tilde{\mathcal{M}}_{n,\beta}$ decreases from its saddle-node tangency to its prefixed critical orbit configuration. The effect of increasing n in the formula for the maps $\tilde{\mathcal{M}}_{n,\beta}$ is to make the corresponding unimodal maps steeper. See Fig. 6. Let $\beta^{sn}(n)$ and $\beta^{pf}(n)$ be the respective saddle-node and prefixed bifurcation β values for each n. The increasing steepness of the graphs as n increases causes the length of the invariant interval $I^{n,\beta^{pf}(n)}$, at the corresponding prefixed bifurcation point for each n, to shrink to zero. The critical value, however, is independent of n: $c_2^{n,\beta} = 2|\beta|(1+\cos(\phi))$. Consequently, as $|\beta|$ decreases, the critical value decreases at the same rate for any n. This combination forces the length of $[|\beta^{pf}(n)|, |\beta^{sn}(n)|]$ shrink to zero as $n \to \infty$. Actually, both

$|\beta^{pf}(n)|$ and $|\beta^{sn}(n)|$ approach the same point on the limiting parabola $\frac{1}{2(1+\cos(\phi))}$ as n increases. See Fig. 5. We conclude that *all* the bifurcation curves inside the parabolic strip approach (pointwise) this same limiting parabola as $n \to \infty$. This justifies our use of the "parabolic strip" terminology.

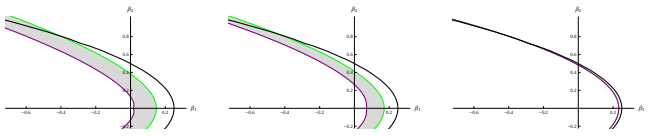

a) n=3 b) n=4 c) n=20

Fig. 5. Graph of parabolic strip boundaries in the β plane: right saddle-node boundary $SN1_n$ (green), left prefixed critical point boundary $PF1_n$ (purple) for $n = 3, 4, 20$. The of the strips shrinks to zero as $n \to \infty$; both left and right boundaries approach the limiting black parabola. By $n = 20$, the strip is too thin to distinguish the boundary curves from each other, and both curves are very close to the limiting parabola.

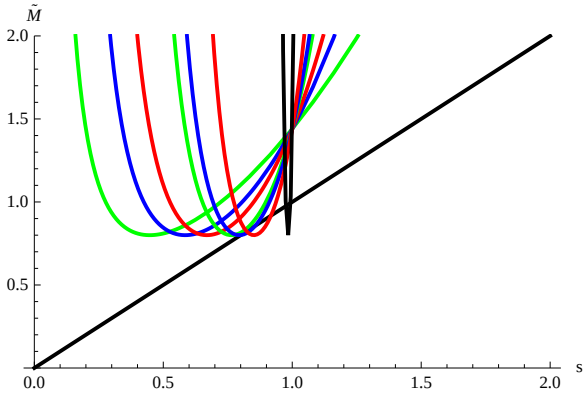

Fig. 6. Graph of $\tilde{\mathcal{M}}_{n,\beta}(s)$ versus s for $\beta = 0.25$, and n varying: 2 (green), 3 (blue), 4 (red), 6 (green), 7 (blue), 10 (red), 100 (black). The "width" of the unimodal maps narrows to zero as $n \to \infty$. All graphs pass through $(s, \tilde{\mathcal{M}}_{n,0.25}(s)) = (1, 1\frac{9}{16})$

3.1.3. *The β parameter plane for $n = 2$.*

The topology of the parabolic strip and its bifurcation curves in the β plane for $n = 2$ is identical to the topology of the strips and curves for $n > 2$ except for one point: the origin. The origin is in the strip since the critical point $s = 0$ for $\tilde{\mathcal{M}}_{2,0}(s) = s^2$ is fixed and therefore bounded. The critical orbit for $\beta = 0$ is fixed at $p_-^{2,0} = 0$; it does not land on $p_+^{2,0} = 1$ on the second iterate as is the case for all other maps on the left-hand boundary of the strip. This "inconsistency" is possible because the family of maps $\tilde{\mathcal{M}}_{2,\beta}$ has a discontinuity when both s and β are zero: $\tilde{\mathcal{M}}_{2,\beta}(0) = \infty$ for $\beta \neq 0$, but $\tilde{\mathcal{M}}_{2,0}(0) = 0$.

All other bifurcation curves (SNk_2, PDk_2, SAk_2, PFk_2) pass through the strip smoothly, but the geometry of the bifurcation curves near the origin is clearly different from the $n > 2$ cases. Although it is not clear from Fig. 7, all the bifurcation curves except $PF1_2$ cross the β_1 axis with positive β_1 value. We justify this statement below, with both numerical continuation and analytic arguments. Another way of stating these results is: any path through the $n = 2$ parabolic strip from right to left that does not pass through the origin is a "full family" (that is, contains all bifurcations present in $x^2 + c$ for $c \in [-2, .25]$). If the path exits through the origin, it contains all bifurcations except the prefixed bifurcation corresponding to $c = -2$. These statements are justified by the following Proposition.

Proposition 2. *Consider the $\beta = |\beta|e^{i\phi}$ parameter plane for the maps $\tilde{\mathcal{M}}_{2,\beta}$ defined in eq. (5). Let PS_2 be the set of all parameter values for which the critical orbit stays bounded.*

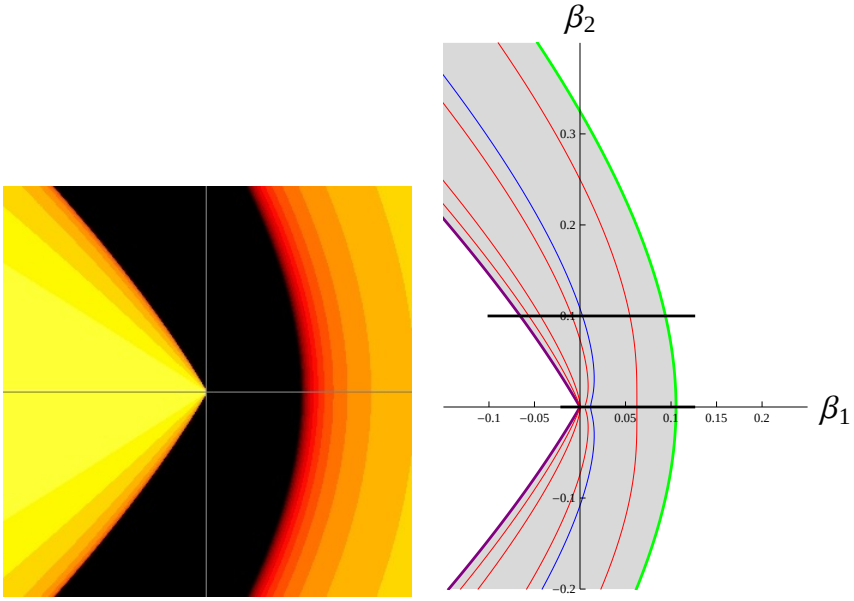

a) b)

Fig. 7. The β parameter plane for $n = 2$. a) colored by escape times; black denotes bounded critical orbit. b) bifurcation curves through the parabolic strip: right to left: fixed-point saddle-node $SN1_2$ (green), superattracting fixed point $SA1_2$ (red), fixed point period-doubling (blue), superattracting period-2 $SA2_2$ (red), superattracting period-3 $SA3_2$ (red), superattracting period-4 $SA4_2$ (red), prefixed critical orbit $PF1_2$ (cyan). The two black line segments at $\beta_2 = 0$ and $\beta_2 = 0.1$ correspond to the one-parameter orbit diagrams in Fig. 9.

(1) Along constant ϕ rays:

(a) If $\phi = \pi$, $\beta \notin PS_2$.

(b) If $\phi \in [-\frac{2\pi}{3}, \frac{2\pi}{3}]$, then for all sufficiently small $|\beta|$, $\beta \in PS_2$.

(c) If $\phi \in (\frac{2\pi}{3}, \frac{4\pi}{3})$, then for all sufficiently small $|\beta|$, $\beta \notin PS_2$.

(2) Along each constant ϕ ray with $\phi \neq \pi$ is a sequence of parameters $\beta^1, \beta^2, ..., \beta^q, ...$ corresponding to superattracting period-q orbits, SAq_2, with $|\beta^1| > |\beta^2| > ... > |\beta^q| > ... > 0$. These superattracting period-q orbits have itineraries $\overline{CLR^{q-2}}$.

(3) For fixed $\phi \neq \pi$, there is a (saddle-node) parameter value $\beta^{sn} = |\beta^{sn}|e^{i\phi}$, satisfying $|\beta^{sn}| > |\beta^q|$ for all q, for which $\tilde{\mathcal{M}}_{2,\beta}$ has a neutral fixed point with derivative one.

(4) For fixed $\phi \in (\frac{2\pi}{3}, \frac{4\pi}{3})\backslash\{\pi\}$ there is a $\beta = \beta^{pf}$ satisfying $0 < |\beta^{pf}| < |\beta_q|$ for all natural numbers q for which the critical orbit is prefixed at p_+^β after two iterates. For $\phi \in [\frac{-2\pi}{3}, \frac{2\pi}{3}]$ there is no β for which the critical orbit is prefixed at p_+^β. The set of all such points $\beta = \beta^{pf}(\phi)$ for $\phi \in (\frac{2\pi}{3}, \frac{4\pi}{3})\backslash\{\pi\}$, together with the origin, forms the left-hand boundary of PS_2.

Proof.

(1) The proofs depend on inspection of the first two iterates of the critical point, given in eq. (6). When the critical value c_1^β is less than the critical point c_0^β, then p_+^β exists. When the second iterate of the critical point, c_2^β, is less than or equal to the fixed point p_+^β, $\beta \in PS_2$; if $c_2^\beta > p_+^\beta$, then $\beta \notin PS_2$.

(a) If $\phi = \pi$, then $c_1 = 0 < c_0 = \sqrt{|\beta|}$, and $c_2^\beta = \infty > p_+^\beta$, and the critical orbit escapes.

(b) Fix $\phi \in [0, \frac{2\pi}{3}]$. Once the result is established for these ϕ, symmetry will automatically give the result for $\phi \in [-\frac{2\pi}{3}, 0)$. If $\phi = 0$, the second iterate of the critical point is $c_2^\beta = 16\beta_1^2 + 2\beta_1 + \frac{1}{16}$ which approaches $\frac{1}{16}$ as $|\beta| \searrow 0$. Meanwhile, the fixed point p_+^β approaches 1. So for sufficiently small $|\beta|$, $c_2^\beta < p_+^\beta$. If $\phi \neq 0$, the second iterate c_2^β approaches $\frac{1}{4(1+\cos(\phi))^2}$ which is still less than 1 provided $\phi \in [0, \frac{2\pi}{3})$. For $\phi = \frac{2\pi}{3}$, c_2^β limits to one, but the limit is approached from below (set

$\phi = \pm\frac{2\pi}{3}$ in eq. (6) to get $c_2^\beta = |\beta| - |\beta|^2 + 1)$, and the right hand fixed point approaches 1 from above (since $\tilde{\mathcal{M}}_{2,\beta}(1) = 1 - |\beta| + |\beta^2|$ is less than one for small $|\beta|$, p_+^β must be greater than one.) So for sufficiently small $|\beta|$, $c_2^\beta < p_+^\beta$.

(c) Fix $\phi \in (\frac{2\pi}{3}, \pi)$. the second iterate c_2^β approaches $\frac{1}{4(1+\cos(\phi))^2}$ which is now greater than one, so for sufficiently small $|\beta|$, $c_2^\beta > p_+^\beta$.

(2) For $q = 1$, there is an explicit formula for $|\beta|$ as a function of ϕ (for $\phi \neq \pi$): eq. (7). For $q = 2$, the result can be established using basic calculus techniques to show the graphs of c_0 and c_2 as functions of $|\beta|$ have exactly two positive intersections. The larger corresponds to the superattracting fixed critical orbit, and the smaller must be the (unique) superattracting period-2. Details are left to the reader. We will use induction to establish the result for $q > 2$.
Assume the result is true for $q = N \geq 2$. Then there is a parameter value β^N for which the critical orbit is period-N. For any β, denote the critical point by $c_0^\beta = \sqrt{|\beta|}$, and its iterates by c_i^β. Since $\tilde{\mathcal{M}}_{2,\beta^N}$ has a periodic critical oribt, it must be true that $\tilde{\mathcal{M}}_{2,\beta}(s) < s$ for all $s \in [c_0^{\beta^N}, p_+^{\beta^N}]$. In particular, this inequality must be true for all points on the critical orbit with itinerary R. Then the points on the critical oribit must be ordered $c_1^{\beta^N} = c_{N+1}^{\beta^N} < c_0^{\beta^N} = c_N^{\beta^N} < c_{N-1}^{\beta^N} < ... < c_3^{\beta^N} < c_2^{\beta^N}$. Therefore, $\tilde{\mathcal{M}}_{2,\beta^N}^{N+1}(c_0^{\beta^N}) = c_1^{\beta^N}$ so $\tilde{\mathcal{M}}_{2,\beta^N}^{N+1}(c_0^{\beta^N}) < c_0^{\beta^N}$. On the other hand, as $|\beta| \searrow 0$, $c_2^\beta \to \frac{1}{4(1+\cos(\phi))^2}$, and $\tilde{\mathcal{M}}_{2,\beta}(s) \to s^2$, so c_N^β approaches $\frac{1}{4(1+\cos(\phi))^{2^N}} > 0$. Meanwhile, $c_0^\beta = \sqrt{|\beta|} \to 0$, so for $\beta = \beta^*$ sufficiently small, $\tilde{\mathcal{M}}_{2,\beta^*}^{N+1}(c_0^{\beta^*}) = c_{N+1}^{\beta^*} > c_0^{\beta^*}$. This forces the order of the beginning of the critical orbit – which need not be periodic – to be $c_1^{\beta^*} < c_0^{\beta^*} < c_{N+1}^{\beta^*} < c_N^{\beta^*} < ... < c_3^{\beta^*} < c_2^{\beta^*}$.
The intermediate value theorem now guarantees the existence of a β^{N+1} with $0 < |\beta|^* < |\beta^{N+1}| < |\beta^N|$ for which the $c_{N+1}^{\beta^{N+1}} = c_0^{\beta^{N+1}}$, so the critical orbit is period-$(N+1)$. Numerical evidence suggests that there is a unique such β^{N+1}, but if not, choose β^{N+1} to make $|\beta^{N+1}|$ the smallest such β. The order of $\{c_0^\beta, ..., c_N^\beta\}$ does not change as $|\beta|$ increases from $|\beta^*|$ to $|\beta^{N+1}|$, so we have $c_1^{\beta^{N+1}} < c_0^{\beta^{N+1}} = c_{N+1}^{\beta^{N+1}} < c_N^{\beta^{N+1}} < ... < c_3^{\beta^{N+1}} < c_2^{\beta^{N+1}}$ and therefore at $\beta = \beta^{N+1}$, the critical orbit has (periodic) itinerary $\overline{CLR^{N-1}}$.

(3) The fixed-point saddle-node curve $SN1_2$ is given by the solution to the system $\tilde{\mathcal{M}}_{2,|\beta|e^{i\phi}}(s) = s$ and $\tilde{\mathcal{M}}'_{2,|\beta|e^{i\phi}}(s) = 1$. This pair of equations can be shown to have an explicit parametric solution in terms of the phase variable s. The second equation can be solved for $|\beta|$ as a function of s, and then substituted into the first equation to solve for $\cos(\phi)$ as a function of s: $(|\beta|, \cos(\phi)) = (\sqrt{s^4 - s^3/2}, \frac{3-4s}{\sqrt{16s^2-8s}})$ for $s \in [9/16, \infty)$. (For $s < 9/16$, a solution would require $\cos(\phi) > 1$.) As s increases from $9/16$ toward ∞, $|\beta|$ increases from $27/256$ toward ∞, and $\cos(\phi)$ simultaneously decreases from 1 toward -1. Correspondingly, ϕ increases from 0 toward π. Both functions are monotonic in s. This establishes the result. Note that this computation shows that the green saddle-node curve in Fig. 7b crosses the β_1 axis at exactly $27/256 \approx 0.1$.

(4) For $\phi \in (\frac{2\pi}{3}, \frac{4\pi}{3})\backslash\{\pi\}$, the result is also an immediate consequence of the intermediate value theorem. By the proof of 1(c), sufficiently small $|\beta|$, $c_2^\beta > p_+^\beta$, but for β^n (for any n) $c_2^{\beta^n} < p_+^{\beta^n}$. So $c_2^\beta = p_+^\beta$ for some β with intermediate $|\beta|$. For $\phi \in [\frac{-2\pi}{3}, \frac{2\pi}{3}]$, the proof of 1(b) shows $c_2^\beta < p_+^\beta$, so we never get a prefixed point, which would require $c_2^\beta = p_+^\beta$, along these rays.

■

This proposition has the following consequences.

Topology: Proposition 2 indicates that the topology of PS_2 is identical to that of PS_n for all other n values, with the exception of one point: the map corresponding to the origin in PS_2 does not correspond to the PF_n point in PS_n on the β_1 axix for $n > 2$. This claim is a corollary of the proposition by noting that continuously varying one-parameter families of unimodal maps are "full families" if they include both a

saddle-node map and a prefixed critical orbit. Continuity guarantees the existence of all "in between" maps. (There is an ordering on the itineraries of critical orbits which we will not define here. See, for example, the discussion on kneading sequences in [Devaney, 1986].) In terms of critical itineraries, these itineraries vary from $C\overline{R}$ (the fixed-point saddle-node itinerary) through $CL\overline{R}$ (the prefixed itinerary). Continuity guarantees all critical itinieraries in between. Since the critical itineraries $\overline{CLR^{q-2}}$ limit to $CL\overline{R}$, then, by continuity, all itineraries in a full family are realized execept $CL\overline{R}$ itself. Numerical investigation suggests that the critical itineraries vary monotonically with respect to this critical itinerary along any ray, be we have not proved this. Itineraries also appear numerically to vary monotonically along constant β_2 lines. They also vary monotonically along constant $|\beta|$ circles since changing ϕ only changes $\tilde{\mathcal{M}}_{n,|\beta|e^{i\phi}}$ by a constant. In terms of conjugacies with x^2+c, in crossing PS_n in any of these three types of paths, there exists a parameter space map $c=h(\beta)$ (which we conjecture can be made one-to-one) for which $\tilde{\mathcal{M}}_{2,\beta}$ is congugate to $x^2+h(\beta)$.

Geometry: The results in part (1) of Prop. 2 are consistent with the numerical continuations which show the left boundary of the parabolic strip PS_2 approaching the origin tangent to $\phi=\pm\frac{2\pi}{3}$. The nearby bifurcation curves SAq_2 all come from the second quadrant into the first, and then swing back toward the origin, crossing the β_1 axis with positive β_1 value, as guaranteed by Prop. 2, part (2). This is evident in Fig. 7b from the two "middle" curves, $SA1_2$ and $PD1_2$. It is evident for $SA3$ and $SA4$ only in the enlargements of Fig. 8. The curves in these enlargements are obtained as an approximation to the SAq_2 curves by looking more carefully at the proof of 1(b). We noticed there that, for $\phi\in[0,\frac{2\pi}{3})$, c_2^β approaches $\frac{1}{(2(1+\cos(\phi)))^2}$, as $|\beta|\searrow 0$. Since $\tilde{\mathcal{M}}_{2,0}(s)=s^2$, $c_k^\beta\approx\frac{1}{(2(1+\cos(\phi)))^{2^{k-1}}}$ for $k\geq 2$. Using $c_0=\sqrt{|\beta|}$, $c_0=c_k$ leads to $|\beta|\approx\frac{1}{(2(1+\cos(\phi)))^{2^k}}$ for $k\geq 2$, although we have not formally justified this approximation.

Scaling of the orbit diagrams. The locations of the superattracting curves SAq_2 in the parabolic strip means that the standard orbit diagrams that one can compute in passing from right to left across the parabolic strip PS_2 have a different scaling at the left-hand boundary, depending on whether the path across the strip passes through the origin. More specifically, the spacing of the superattracting curves SAq_2 near the left hand boundary is asymptotically linear for curves not passing through the origin, with constant which can be shown to be equal to the reciprocal of the eigenvalue λ of the fixed point $p_+^{n,\beta^{PF}}$. That is, $\frac{|\beta^{n+1}-\beta^n|}{|\beta^n-\beta^{n-1}|}\to 1/\lambda$. This convergence, however, is asymptotically quadratic for curves passing through the origin. Compare the two orbit diagrams for two horizontal slices, one which goes through the origin ($\beta_1=0$), and one which doesn't ($\beta_1=0.1$) in Fig. 9. In Fig. 9a, width of the whole diagram is approximately 0.1, but the period-3 superattracting parameter value is $\beta_1\approx 1.5\times 10^{-5}$, so the usual orbit diagram from the usually prominent period-3 window through the prefixed critical orbit parameter value, is compressed into this tiny interval, and therefore not really visible at all. In Fig. 9b, the orbit diagram appears more typical, with the usually prominent period three window clearly visible.

3.1.4. *The β parameter plane for $n=1$.*

The maps are still unimodal and $\tilde{\mathcal{M}}_{1,\beta}(s)=s+2|\beta|\cos(\phi)+\frac{|\beta|^2}{s}=s+2\beta_1+\frac{|\beta|^2}{s}$ is still negative Schwarzian. Infinity is still a fixed point, but the escape criterion in Theorem 1 does not apply; the derivative at infinity is zero: infinity is weakly attracting if $\beta_1\geq 0$ (that is, $\phi\in[-\pi/2,\pi/2]$), but weakly repelling if $\beta_1<0$. The companion point $\tau(\infty)=0$ since $\tilde{\mathcal{M}}_{1,\beta}(0)=\infty$ for $\beta\neq 0$.

Maps along rays from the origin in the β plane are all conjugate: the rescaling $u=s/|\beta|$ conjugates $\tilde{\mathcal{M}}_{n,|\beta|\cos(\phi)}$ to $\tilde{\mathcal{M}}_{n,\cos(\phi)}$, so all bifurcation curves are rays from the origin as well. The bifurcation curves in the β parameter space are analogous to those for $n>1$, with some minor adjustments in interpretation, like thinking of the fixed point at infinity as a finite fixed point. If $\beta_1>0$, then $\tilde{\mathcal{M}}_{n,\beta}(s)>s$ for all s, and all orbits escape to infinity; no finite fixed point exists. If $\beta_1<0$, then there is a unique finite fixed point at $s=-\frac{\beta_1^2+\beta_2^2}{2\beta_1}=p_-$, while ∞ more naturally corresponds to p_+. For $n=1$, following the unit circle in the β plane from $\phi=\pi/2$ to π corresponds to crossing the parabolic strips for $n>1$ from right to left in the upper half plane. The ray $\phi=\pi/2$ corresponds to a saddle-node fixed point (at infinity). This is justified since, as $\phi\to\pi/2^+$, the finite fixed point p_- approaches the "other" fixed point at $p_+=\infty$. The ray

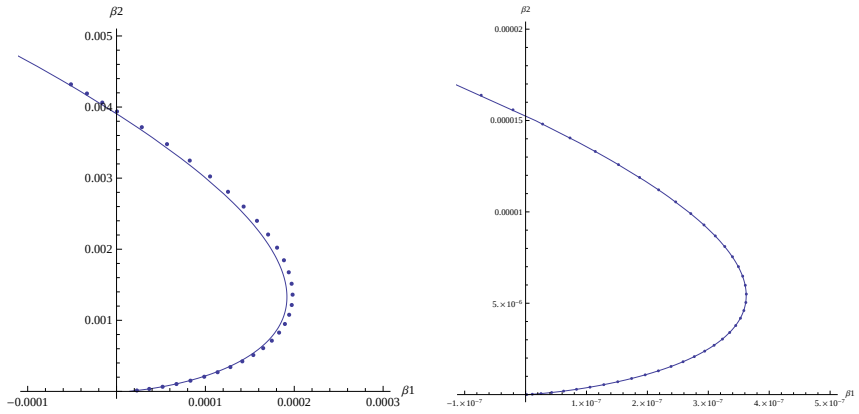

a) Period-3

b) Period-4

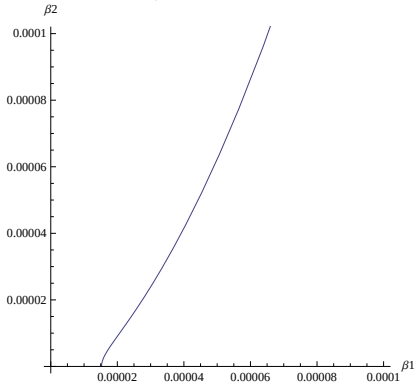

c) Period-3 enlargement

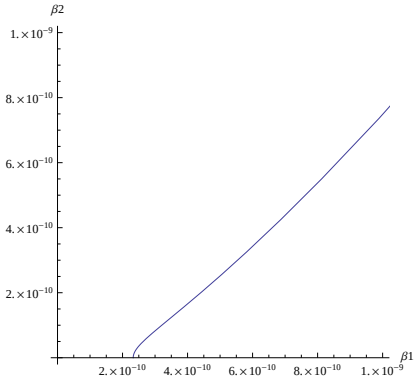

d) Period-4 enlargement

Fig. 8. The geometry of the superattracting period-3 and period-4 curves in the β parameter plane for $n = 2$. Solid lines are the approximations $|\beta| \approx \frac{1}{(2(1+\cos(\phi)))^{2^{k-1}}}$; points in a and b are numerically computed SA_3 and SA_4 points, respectively. We do not show the curves for negative β_2, but recall they are symmetric across the β_1 axis.

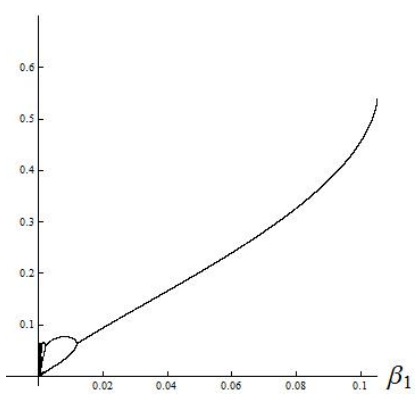

a) $\beta_2 = 0$

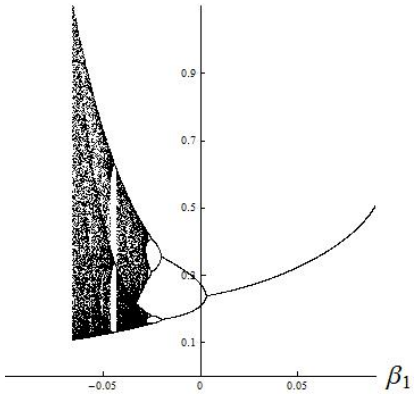

b) $\beta_2 = 0.1$

Fig. 9. Orbit diagrams - s versus β_1 for two one-parameter cuts through PS_2 (for $z^2 + \beta/\bar{z}^2$). See black line segments corresponding to these one-parameter cuts in Fig. 7. a) the orbit diagram along the β_1 axis is extremely "compressed" toward the left side, b) the orbit diagram looks more "standard", like the orbit diagram for $x^2 + c$.

$\phi = 2\pi/3$ has superattracting fixed points. The ray $\phi = 3\pi/4$ has the period-doubling fixed points (with eigenvalue negative one). The ray $\phi = \pi$ corresponds to a critical orbit which is fixed (at infinity) after two iterates: $|\beta| \mapsto 0 \mapsto \infty$. As for all n, the symmetry of the β plane requires complex conjugate parameter values to have dynamically conjugate behavior. The "Cantor set region," to the left of the parabolic strips

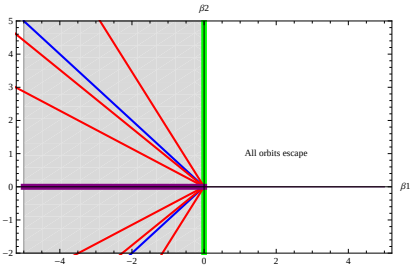

Fig. 10. The parameter plane for $n = 1$. Bifurcation curves are all rays from the origin. The "parabolic strip" is the left half plane. Bifurcation curves counterclockwise through the second quadrant: fixed point period-doubling (blue), fixed-point saddle-node $SN1_1$ (green), superattracting fixed point $SA1_1$ (red), superattracting period-2 $SA2_1$ (red), superattracting period-3 $SA3_1$ (red), superattracting period-4 $SA4_1$ (red), prefixed critical orbit (at infinity) $PF1_1$ (cyan).

for $n > 1$, does not exist at all for $n = 1$.

3.1.5. *Modulus Map Dynamics*

The dynamics of unimodal maps is nontrivial, but well-established, especially since there are no wandering intervals (guaranteed by being negative Schwarzian). We provide only a limited summary here. See [Guckenheimer J, 1979; de Melo & van Strein, 1993], for example, for details.

For parameter values to the right of the parabolic strips (for $n \geq 2$), all orbits escape to infinity. For parameter values to the left of the strip, where the set of bounded orbits is a (measure zero) Cantor set, the dynamics is equivalent to the full shift on two symbols. For parameter values in the parabolic strip, the bounded set is the invariant interval, $I^{n,\beta} = [\tau(p_+^{n,\beta}), p_+^{n,\beta}]$, and unimodal map results [de Melo & van Strein, 1993] guarantee the radial map dynamics has one of three transitive topological attractor types: periodic, Cantor set (at the 'Feigenbaum parameter values'), or a finite union of intervals (at parameter values where the critical orbit is preperiodic). (De Melo and van Strein [1993] define a set $A \subset I^{n,\beta}$ to be a *topological attractor* if it is forward invariant, $cl(B(A))$ contains intervals, and $cl(B(A))\backslash cl(B(A'))$ contain intervals whenever A' is a forward invariant set strictly contained in A. The basin $B(A)$ is the set of all points in I whose omega limit set is contained in A.) In this classification, saddle-node bifurcation points and period-doubling points, as well as parameter values corresponding to hyperbolic periodic orbits, are included in the 'periodic attractor' parameter set. The attractor in the 'finite union of intervals' set admits chaotic dynamics, with transitive behavior and a dense set of periodic points; the dynamics is a generalized version of the chaotic dynamics present for $x^2 - 2$ on $[-2, 2]$. The dynamics on the attracting Cantor set is conjugate to an "adding machine." (Note that this dynamical description is quite different from dynamics on the Cantor set for parameter values to the left of the parabolic strips.) The attracting Cantor set is known to be a minimal set, with no closed, invariant subsets. In particular, there exist no periodic orbits. So the dynamics is transitive, but clearly without a dense set of periodic points. Using the definition of chaotic dynamics as being both transitive and having a dense set of periodic points with more than one periodic orbit, only the finite union of intervals case admits chaotic behavior.

3.2. *Full dynamics in the plane*

We finally are ready to address on of the main goals of the paper: describing the dynamics of the full planar map $P_{n,\beta}$ of eq. (4). The behavior of the modulus map $\mathcal{M}$ (or its conjugate $\tilde{\mathcal{M}}$) completely determines the orbits which are bounded versus escape orbits for $P_{n,\beta}$. It also gives a lot of information about the dynamics of the bounded orbits as well. To understand the full planar dynamics, we need to look more closely at the angular map $\mathcal{A}_{n,\beta}$, defined in eq. (4) as $\mathcal{A}_{n,\beta}(\theta) = n\theta + Arg\left(r^n + \frac{\beta}{r^n}\right)$. (Since we have established the dynamics of the radial map $\mathcal{M}$ via its conjugate $\tilde{\mathcal{M}}$, we return to using the original map, $\mathcal{M}$ to describe the full planar dynamics. To obtain the correponding results in terms of the conjugate map $\tilde{\mathcal{M}}$, the variable r can be replaced by $s^{1/2}$.) Although this map is dependent on both r and θ, the dependence on r is in

a simple way. Denoting the k^{th} iterate of the radial map $\mathcal{M}$ by r_k, it is easy to show that the angular coordinate of the k^{th} iterate of the full planar map has the following formula:

$$\theta_k \equiv \mathcal{A}^k_{n,\beta}(\theta_0) = n^k\theta_0 + \sum_{i=0}^{k-1} n^i Arg\left(r_{k-1-i} + \frac{\beta}{r^n_{k-1-i}}\right) \tag{8}$$

Since r_i is independent of θ, the k^{th} iterate of the angular map merely sends θ to $n^k\theta$ plus a radially dependent translation. This translation is zero when β is real and positive. The proofs establishing that certain of the $P_{n,\beta}$ maps are chaotic turn out to be only marginally more difficult than showing that $\theta \mapsto n\theta$ is chaotic as a map of $\mathbb{S}^1$. More specifically, we have the following lemma.

Lemma 1. *Assume the orbit of r_0 is bounded under iteration by $\mathcal{M}_{n,\beta}$. Consider the arc $S = \{r_0\} \times (\theta_0 - \epsilon, \theta_0 + \epsilon)$ for any fixed $\epsilon > 0$. There exists a $K \in N$ such that for all $k \geq K$, $P^k_{n,\beta}(S)$ is a full circle in the plane.*

Note: We restrict to bounded orbits primarily to make sure that $r_k \neq 0$ or ∞.

Proof. Choose K sufficiently large that $2n^K\epsilon > 2\pi$. By the independence of the radial component (eq. (4)), arcs of circles centered at the origin map to arcs of new circles centered at the origin. By the form of eq. (8), the choice of K ensures the angular length (in $\mathbb{R}$) of $P^k_{n,\beta}(S)$ is greater than 2π. Then $k \geq K$, along with $r_k \neq 0, \infty$, implies the arc is a full circle in the plane: $P^k_{n,\beta}(S) = \{r_k\} \times \mathbb{S}^1$. ■

We use this lemma to prove the next three propositions, which connect the dynamics of the radial map $\mathcal{M}$ to the full planar map P.

Proposition 3. *If a subset $A \subset (0, \infty)$ is (forward) invariant under $\mathcal{M}_{n,\beta}$, then $\{(r, \theta) \in A \times \mathbb{S}^1\}$ is (forward) invariant under $P_{n,\beta}$.*

Proof. This is automatic since the modulus map $\mathcal{M}_{n,\beta}$ is independent of θ. ■

Recall the definition of $f : X \to X$ being it transitive: Given $x \in X$, $y \in X$ and $\epsilon > 0$, there exists a $z \in X$ and $N \in \mathbf{N}$ such that $d(x, z) < \epsilon$ and $d(f^N(x), y) < \epsilon$. Note that the N can be assumed to be arbitrarily large; see [Akin, 1993], for example.

Proposition 4. *If $\mathcal{M}_{n,\beta}$ is transitive on a subset $A \subset (0, \infty)$, then $P = P_{n,\beta}$ is transitive on the subset of the plane: $\{(r, \theta) \in A \times \mathbb{S}^1\}$.*

Proof. In this proof, d_1 and d_2 will be the usual Euclidean metrics in $\mathbb{R}^1$ and $\mathbb{R}^2$, respectively. Let (r_0, θ_0) and (r_1, θ_1) be arbitrary points in $(0, \infty) \times \mathbb{S}^1$. Let $\epsilon > 0$ be given. We must find a third point (r', θ') that is near (r_0, θ_0) and iterates near (r_1, θ_1). The idea is to use the transitivity of the modulus map to find an r' is near r_0 for which the modulus of some iterate N of (r', θ') is near r_1, and use Lemma 1 to find a θ' near θ_0 for which the angular component of the Nth iterate of (r', θ') matches θ_1 exactly. Details follow. Choose a "polar coordinate neighborhood" of (r_0, θ_0) that is contained in an ϵ ball (in $\mathbb{R}^2$) around (r_0, θ_0), denoted $B_\epsilon(r_0, \theta_0)$. That is, choose $\epsilon_r > 0$ and $\epsilon_\theta > 0$ such that $W = (r_0 - \epsilon_r, r_0 + \epsilon_r) \times (\theta_0 - \epsilon_\theta, \theta_0 + \epsilon_\theta) \subset B_\epsilon(r_0, \theta_0)$. See Fig. 11. Note that this requires $\epsilon_r < \epsilon$. Now choose K as in Lemma 1 for ϵ_θ. Use the transitivity of $\mathcal{M}$ along with an "epsilon" of ϵ_r to find a radius r' and N satisfying $d_1(r', r_0) < \epsilon_r$, and $d_1(\mathcal{M}^N(r'), r_1) < \epsilon_r$. As mentioned in the note following the definition of transitive above, we can assume $N \geq K$. Lemma 1 now guarantees that $P^N(\{r'\} \times (\theta_0 - \epsilon_\theta, \theta_0 + \epsilon_\theta))$ is a circle. Thus, there exists a $\theta' \in (\theta_0 - \epsilon_0, \theta_0 + \epsilon_0)$ such that $P^N(r', \theta')$ $= (\mathcal{M}^N(r'), \theta_1)$. That is, $(r', \theta') \in W \subset B_\epsilon(r_0, \theta_0)$, and $d_2(P^N(r', \theta'), (r_1, \theta_1)) = d_1(\mathcal{M}^N(r'), r_1) < \epsilon_r < \epsilon$. ■

Proposition 5. *If $\mathcal{M}_{n,\beta}$ has a dense set periodic points in $A \subset (0, \infty)$, then $P_{n,\beta}$ has a dense set of periodic points in the subset of the plane: $\{(r, \theta) \in A \times \mathbb{S}^1\}$.*

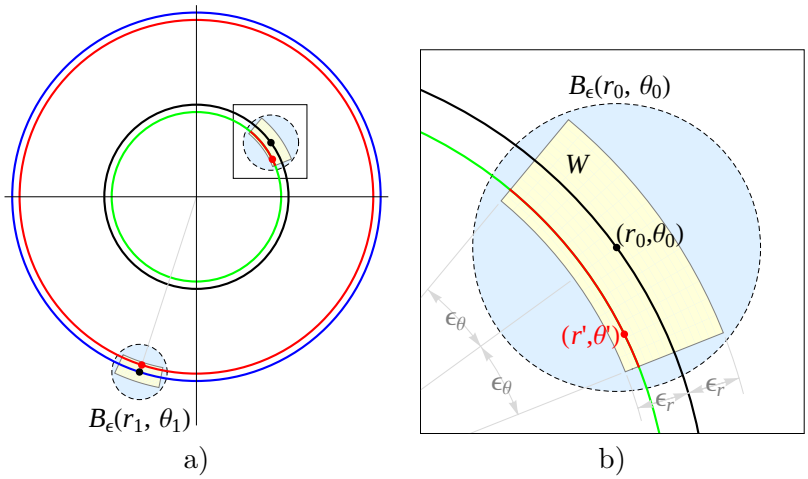

Fig. 11. Figure to accompany the proof of Proposition 4: transitivity in the modulus map implies transitivity in the plane. a) full phase plane. b) enlargement of one neighborhood. The orbit of (r', θ') starts near (r_0, θ_0) and lands near (r_1, θ_1). The unlabelled red point near $((r_1, \theta_1)$ is $P^N(r', \theta')$; its angle matches θ_1 exactly. The labels in the enlargement on the right match the notation used in the proof of Proposition 4.

Proof. The method of proof is almost identical to the proof of transitivity in the preceding proposition. Given a point (r_0, θ_0), we use the denseness of periodic points for $\mathcal{M}$ to find a period-q r' value near r_0, and iterate a small arc with radius r' a sufficient number of multiples of q to ensure the image is a circle. This ensures that we can match the angular component after $N = kq$ iterates for some k. Details are left to the reader. ■

Dynamical consequences for $P_{n,\beta}$. The combination of the unimodal map results for $\mathcal{M}$ (equivalently $\tilde{\mathcal{M}}$), along with the above three propositions, gives the following dynamical description for the family of nonholomorphic, singular maps of the plane, $P_{n,\beta}$.

Fix an integer $n \geq 1$. Consider the β parameter plane for $\mathcal{M}_{n,\beta}$ for this n. Then the full planar maps $P_{n,\beta}$ have the following behavior. The set with bounded orbits, $K(P_{n,\beta}) = K(\mathcal{M}_{n,\beta}) \times \mathbb{S}$, and its boundary $J(P_{n,\beta}) = J(\mathcal{M}_{n,\beta}) \times \mathbb{S}$.

Recall the set of parameters, PS_n, for which $\tilde{\mathcal{M}}_{n,\beta}$ has a bounded critical orbit.

(1) If β is to the right of PS_n, then all orbits escape to infinity. In particular, $K(P_{n,\beta}) = J(P_{n,\beta}) = \phi$. Note that an empty bounded orbit set is not possible for complex rational maps of $\hat{\mathbb{C}}$.

(2) If β is to the left of PS_n (this set is empty for $n = 1$), then all orbits escape to infinity except for $K(P_{n,\beta}) = J(P_{n,\beta})$, a Cantor set of circles. The dynamics restricted to $K(P_{n,\beta})$ is transitive and has dense periodic points, and therefore is chaotic. There is no attractor in any topological or measure sense. (The Cantor set in the line has measure zero [de Melo & van Strein, 1993], so the Cantor set of circles has zero measure in the plane. All other orbits escape. The (closure of) the basin, therefore, has zero measure.

(3) If $\beta \in PS_n$, then $K(P_{n,\beta}) = I^{n,\beta} \times \mathbb{S}$, an annulus in the plane, and $J(P_{n,\beta}) = \left(\{p_+^{n,\beta}\} \bigcup \{\tau(p_+^{n,\beta})\}\right) \times \mathbb{S}$, the union of two circles in the plane. The inner circle $\{\tau(p_+^{n,\beta})\} \times \mathbb{S}$ maps to the outer circle $\{p_+^{n,\beta}\} \times \mathbb{S}$, which is fixed. The propositions guarantee that $P_{n,\beta}$ restricted to this outer circle is transitive and has a dense set of periodic points, and is therefore chaotic. The description of the dynamics of $P_{n,\beta}$ restricted to $K(P_{n,\beta})$ breaks up into three cases, corresponding to the three subcases for the unimodal modulus map when the critical orbit is bounded.

   (a) When the attractor A for $\mathcal{M}_{n,\beta}$ periodic, then $A \times \mathbb{S}$ is an attractor for $P_{n,\beta}$, and the dynamics restricted to this finite union of circles is transitive and has dense periodic points, and therefore chaotic.

   (b) When the attractor A for $\mathcal{M}_{n,\beta}$ a Cantor set, then $A \times \mathbb{S}$ is an attractor for $P_{n,\beta}$, and the dynamics restricted to this Cantor set of circles is transitive. There are no periodic points.

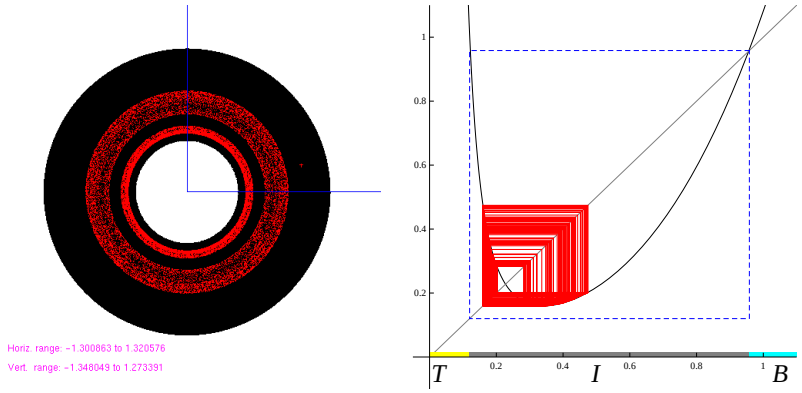

a) b)

Fig. 12. a) Dynamic space for $z^3 + 0.04/\bar{z}^3$. Bounded orbits are in black; the attractor is in red. The initial condition for the red orbit is indicated by the plus in the first quadrant. b) corresponding graphical iteration for $\tilde{\mathcal{M}}_{3,0.04}$.

(c) When the attractor A for $\mathcal{M}_{n,\beta}$ a finite union of intervals, then $A \times \mathbb{S}$ is an attractor for $P_{n,\beta}$, and the dynamics restricted to this finite union of annuli is transitive and has dense periodic points, and therefore chaotic. This case is illustrated in Fig. 12, where A appears to be a union of two intervals (indistinguishable numerically from a high period periodic orbit), and $A \times \mathbb{S}$ appears to be a union of two annuli.

Remarks:

(1) In order to translate the use of the word "attractor" from the one-dimensional unimodal map setting to the two-dimensional setting, we define $A \times \mathbb{S}$ to be an attractor whenever A is an attractor in $\mathbb{R}$. Thus, our two-dimensional attractors have the property (among others) that the closure of their basins of attraction contain open sets.
(2) The two-dimensional periodic attractors which correspond to hyperbolic attracting periodic orbits for the radial map are attractors using even the most stringent definition of attractor: attracting a neighborhood of the attractor. The same is true for nonhyperbolic periodic orbits at the period-doubling points, but at the saddle-node points, the attractors are only one-sided attractors.
(3) Since the one-dimensional attractors A all attract sets of full measure in $K(\tilde{\mathcal{M}}_{n,\beta})$ [de Melo & van Strein, 1993], $A \times \mathbb{S}$ attracts a set of full measure in $K(P_{n,\beta})$ in cases 3(b) and 3(c) above, as well as case 3(a).

3.3. *Comparison with holomorphic singular perturbations*

In this section we compare certain features of the dynamics of $z^n + \frac{\beta}{\bar{z}^n}$ with the corresponding dynamics of its holomorphic analogue, $z^n + \frac{\lambda}{z^n}$.

- Although the parameter plane (β versus λ) and dynamic plane escape diagrams for the holomorphic perturbations and nonholomorphic perturbations are very different, they do share common features. Specifically, along their "real spines" in the parameter planes and restricted to real initial conditions, both maps are the same. This is corroborated in Fig. 13: the restriction of Figs. 13a and 13b to the real axis is the same (two line segments, symmetric about the origin), as is the restriction of Figs. 13c and 13d (two Cantor sets, also symmetric about the origin).
- Similarly, the parameter plane figures for both families agree along the *positive* real axis. See Figs. 14 for $n = 3$ and 15 for $n = 2$, where the real positive β values intersecting the respective parabolic strip matches the real positive λ values intersecting the respective Mandelbrot set. Note that they do not match on the respective negative real axes. This is because for real, negative values of λ, the critical points used to create the λ parameter planes of Figs. 14 and 15 are nonreal. The corresponding maps for β don't even have a critical point. Instead, they have an asymptote at $x = 0$. But the corresponding modulus map has a critical

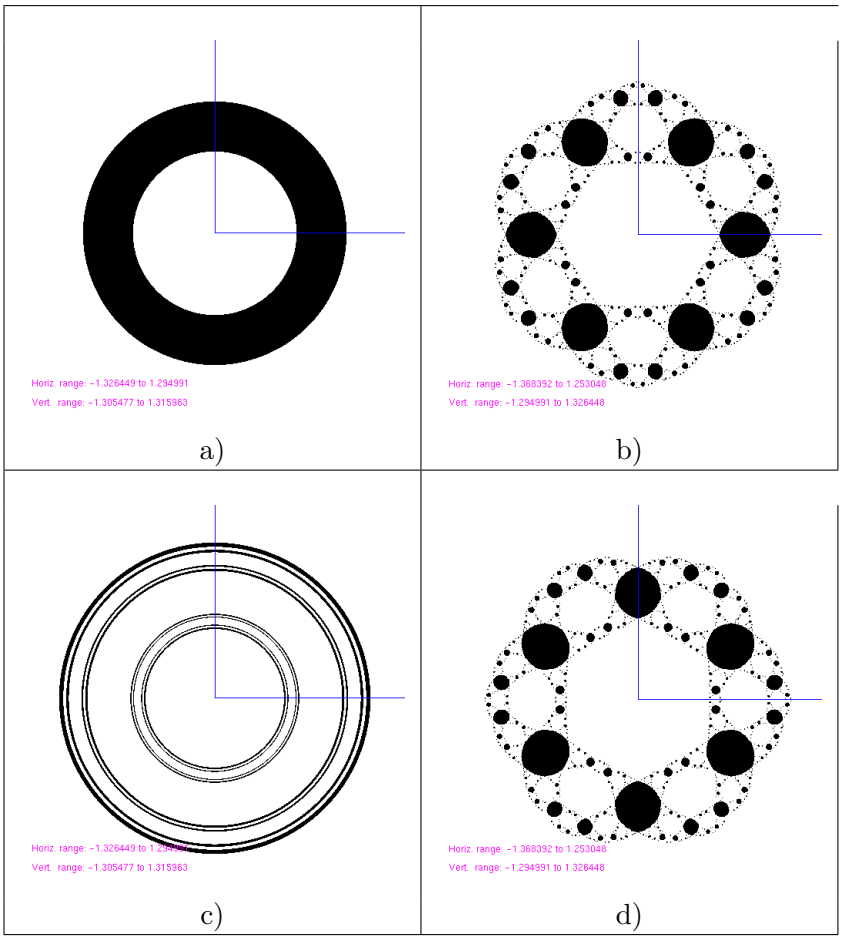

Fig. 13. Dynamic space comparison of nonholomorphic versus holomorphic families for $n = 3$ and analogous "continuation" parameters: a) $\beta = 0.125$ b) $\lambda = 0.125$ c) $\beta = -0.125$ d) $\lambda = -0.125$. Note that the black in figures a and b match along the x axis as two symmetric closed intervals. Figures c and d also match as two symmetric Cantor sets.

point where the critical value is zero. So the starting points for the numerical parameter plane experiments do not match in the β versus λ planes.

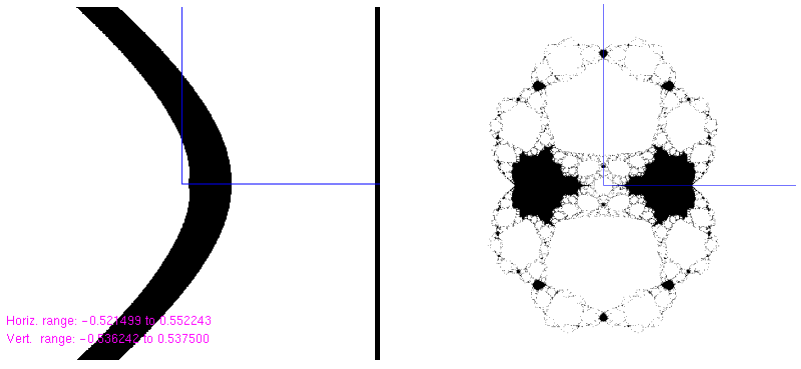

Fig. 14. Parameter plane comparison for $n = 3$. a) $z^3 + \beta/\overline{z}^3$. b) $z^3 + \lambda/z^3$ The black regions match along the *positive* x-axis.

- Note that in all subcases of case 3 above, $J(P_{n,\beta})$ is the union of two circles, and the inner circle maps to the outer circle, on which $P_{n,\beta}$ is chaotic. This differs from the situation with rational holomorphic maps, where the Julia sets are transitive and densely filled with periodic points.

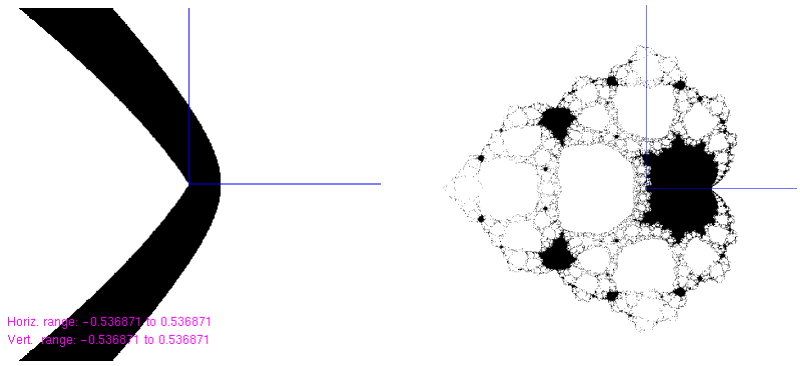

a) β plane b) λ plane

Fig. 15. Parameter plane comparison for $n = 2$. a) $z^2 + \beta/\overline{z}^2$. b) $z^2 + \lambda/z^2$ The black regions match along the *positive* x-axis.

- The critical set of $z^n + \frac{\lambda}{z^n}$ consists of $2n$ points, all on a circle of radius $|\lambda|^{1/2n}$. The critical set of $z^n + \frac{\beta}{\overline{z}^n}$ is a circle of radius $|\beta|^{1/2n}$. What makes both families easier to study is that all critical orbits have similar behavior.
- The quadratic convergence of SAq_2 approaching the origin versus the linear convergence of SAq_n for $n > 2$ is consistent with the different appearances of the Mandelbrot sets for $n = 2$ versus $n > 3$. The set for $n = 3$ looks like a typical Mandelbrot set, while the set for $n = 2$ is distorted near the origin. See Figs. 14 and 15 below. This distortion for $n = 2$ is directly related to the compressed orbit diagram in Fig. 9a since the orbit diagram is taken along the "spine" of the $n = 2$ Mandelbrot set in Figs. 15.
- That the "McMullen domains" (the parameter values for which the corresponding filled Julia set is a Cantor set of circles) exist only for $z^n + \lambda/z^n$ if $n > 2$ [Devaney, 2010] is consistent with the observation that the parabolic strips PS_n lie to the right of the origin for $n > 2$, but include the origin on its boundary for $n = 2$.

4. Generalizations

In the introduction of this paper, we proposed the study of a six-parameter family of rational maps of the plane: $z^n + c + \beta/\overline{z}^d$. We reduced the study to three parameters by setting $c = 0$ and $n = d$. We then fixed n and considered bifurcations in the remaining parameter plane β. The specific famlily on which we chose to focus was guided by a desire to compare and contrast holomorphic rational map behaviors with the behavior of more general maps of the real plane. There are many other reductions and/or generalizations that could have been made. For example, we chose our family from the following larger set of maps: $z^n + c + \frac{\lambda}{z^{d_1}} + \frac{\beta}{\overline{z}^{d_2}} + \alpha\overline{z}$. A natural approach might be to consider any number of these parameters as fixed, or auxiliary parameters, and leave two primary parameters to vary. The primary parameter plane could then be studied as the auxiliary parameters are varied. One major difficulty in such a study is that, in general, the critical set consists of curves, and different points in the critical set can have different behaviors.

We close with a numerical experiment which suggests the complications, and beauty, that might exist in such a study by displaying a parameter space picture for the family $z^2 + \frac{\beta}{\overline{z}^1}$. This family has a critical circle at $|z| = |\beta|^{1/5}$. The coloring scheme was determined by the behavior of three different points on this critical circle, at angles of 0, $2\pi/3$, and $4\pi/3$. The two conjugate parameter values always had the same escape behavior, but their behavior did not have to match the escape behavior for the point on the positive β_1 axis. The coloring scheme was determined by the sum of the escape iterates for all three points.

We plan to study more of these families in the future, classifying the maps by their critical sets and dynamical behavior of their images.

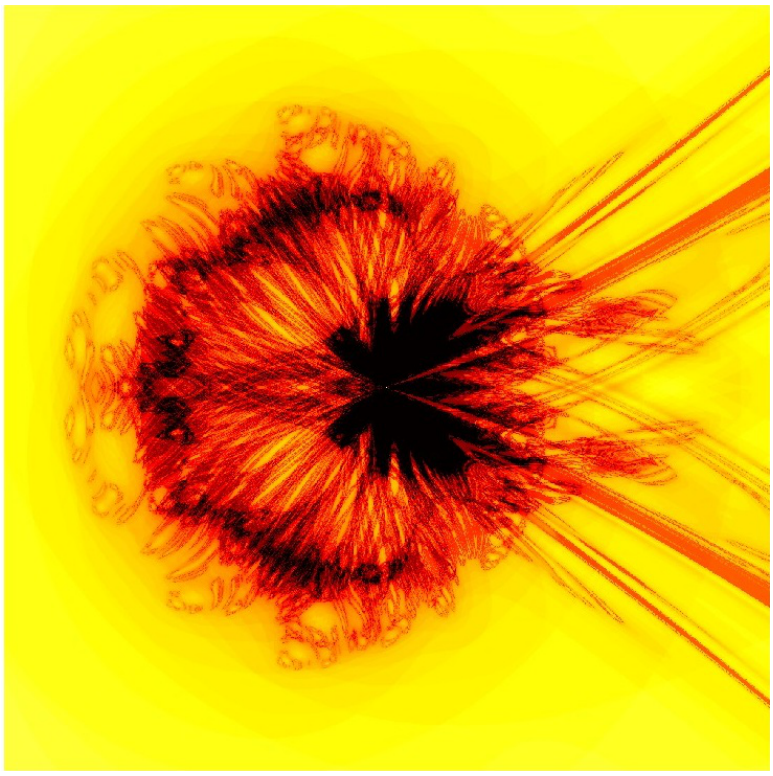

Fig. 16. Beta parameter plane escape experiment for $z^2 + \beta/\bar{z}^1$. Coloring is determined by the sum of the escape "times" for three points on the critical circle.

5. Acknowledgements

The authors would like to thank the following for helpful discussions: Paul Blanchard, Robert Devaney, John Guckenheimer, Roger Kraft, Richard McGehee.

References

Akin E [1993], The general topology of dynamical systems, *Graduate Studies in Mathematics*, Vol. 1, (Providence: AMS).

Blanchard Paul, Cilingir Figen, Cuzzocreo Daniel, Devaney Robert L., Look Daniel M., Russell Elizabeth D. [2012 preprint], "Checkerboard Julia Sets for Rational Maps," submitted to *Int. J. Bifurcation and Chaos*.

Blanchard, Paul, Devaney, Robert L., Look, Daniel M., Seal, Pradipta, Shapiro, Yakov [2005], "Sierpinski Curve Julia Sets and Singular Perturbations of Complex Polynomials," *Ergodic Theory and Dynamical Systems* **25**, 1047-1055.

Bielefeld B., Sutherland S., Tangerman F., Veerman J.J.P. [1993], "Dynamics of Certain Nonconformal Degree-Two Maps of the Plane," *Experimental Mathematics* **2** No. 4, 281-300.

Bozyk B., Non-Analytic Singular Continuations of Complex Analytic Dynamical Systems, Master's thesis, University of Minnesota Duluth, 2012.

Bruin H. and Martijn van Noort, [2004] "Nonconformal perturbations of $z \to z^2 + c$: the 1:3 resonance," *Nonlinearity* 17, 765 - 789.

Devaney, Robert L. [1986], *An Introduction to Chaotic Dynamical Systems*, (Addison-Wesley, New York; second edition 1989, now published by Westview Press Perseus Books Publishing 2003).

Devaney, Robert L. [2010], "Singular Perturbations of Complex Analytic Dynamical Systems," *Nonlinear Dynamics and Chaos: Advances and Perspectives*, Springer-Verlag, Berlin, 13-29.

Devaney, Robert L., [2012], "Dynamics of $z^n + \lambda/z^n$, Why the Case $n = 2$ is Crazy," *Conformal Dynamics and Hyperbolic Geometry*, Contemporary Math. AMS Vol. 573, 49-65.

Devaney, Robert L., Look, Daniel M., Uminsky D [2005], "The Escape Trichotomy for Singularly Perturbed Rational Maps," *Indiana University Mathematics Journal* **54**, 1621-1634.

Drexler J [1996], "A Nonanalytic Perturbation of the Complex Quadratic Family of Maps," Master's Project University of Minnesota, Duluth, Technical Report 96-5.

Guckenheimer J [1979], "Sensitive dependence to initial conditions for one dimensional maps," Commun. Math. Phys. 70, 133-160.

Kraft, R, *Some One-dimensional Dynamics*, preprint, 2012.

De Melo W and van Strein S [1993] *One-dimensional Dynamics*, A Series of Modern Surveys in Mathematics, **3(25)** (Springer-Verlag, Berlin, New York).

Mira C and T. Narayaninsamy [1993], "On two behaviors of two-dimensional endomorphisms: Role of the critical Curves," *Int. J. Bifurcation and Chaos*, Vol. 3, No. 1, 187-194.

Peckham, B B [1998], "Real Perturbations of Complex Analytic Families: Points to Regions," *International Journal of Bifurcation and Chaos*, Vol 8, No. 1, 73-93.

Peckham B B [1988-2012], *To Be Continued ...*, a continuation software package for discrete dynamical systems (continually under development).

Peckham B B and Montaldi J [2000], "Real Perturbation of the complex quadratic familiy: Fixed point bifurcation loci." *International Journal of Bifurcation and Chaos*, Vol 10, No. 2, 391-414.